Submitted for publication in ApJL
Preprint typeset using LaTeX style emulateapj v. 12/16/11

THE PLACE OF THE LOCAL GROUP IN THE COSMIC WEB

J. E. Forero-Romero[1] and R. González[2]
[1] Departamento de Física, Universidad de los Andes, Cra. 1 No. 18A-10, Edificio Ip, Bogotá, Colombia
[2] Instituto de Astrofísica, Pontificia Universidad Católica, Av. Vicuña Mackenna 4860, Santiago, Chile

Submitted for publication in ApJL

ABSTRACT

We explore the characteristics of the Local Group (LG) location in the cosmic web using a cosmological simulation in the ΛCDM cosmology. We use the Hessian of the gravitational potential to define the cosmic web, where regions are classified as either peak, sheet, filament or void. The LG in the simulations are split into two samples. The first is a general sample composed by halo pairs with similar masses and isolation criteria as observed in the LG. The second is a subset with additional kinematic constaints. We find that the pairs in the LG sample with all constraints are: i) Preferentially located in filaments and sheets, ii) located in in a narrow range of local overdensity $0 < \delta < 4$, web ellipticity $0.1 < e < 1.0$ and prolateness $-0.5 < p < 0.5$. iii) Clearly aligned with the cosmic web, in particular for pairs in filaments/sheets the orbital angular momentum tends to be perpendicular to the filament direction or the sheet plane. A stronger alignment is present for the vector linking the two halos, which lies along the filament or the sheet plane. We show that the first and second results are expected trends with the LG total mass. However, the strong alignment with the cosmic web cannot be explained in the same way.

Subject headings: galaxies: Local Group — dark matter

1. INTRODUCTION

The spatial and kinematic configuration of the Local Group (LG) galaxies is rare to find in the local Universe and in cosmological simulations. The LG is dominated by the two big spirals MW and M31, the next most-luminous galaxy is M33 which is ~ 10 times less massive than M31, followed by several less luminous dwarf galaxies, up to a distance of $\sim$ 3Mpc. The velocity vector of M31, with a low tangential velocity is consistent to a head-on collision orbit toward the MW (Cox & Loeb 2008; van der Marel et al. 2012b; Sohn et al. 2012).

Another feature of the Local group is the relatively low velocity dispersion of nearby galaxies up to ~ 8 Mpc (Sandage & Tammann 1975; Aragon-Calvo et al. 2011, and references therein). Environment around the Local Group has density quite close to the average density of the universe (Klypin et al. 2003; Karachentsev 2005). In addition, the closest massive galaxy cluster, the Virgo Cluster, is ≈ 16.5 Mpc away (Mei et al. 2007).

All this combination of features make LG analogues rare to find. Using numerical simulatons González et al. (2013a) found less than 2% MW-sized halos reside in a pair similar to MW-M31 and in a similar environment. Furthermore, if we select pairs constrained within 2σ error fron current observational measurements of the velocity components and distance to M31, there are only 46 systems in a cubic volume of 250 h^{-1}Mpc side, giving a number density $\sim 1.0 \times 10^{-6}$Mpc^3, comparable to the abundance of massive clusters.

Forero-Romero et al. (2013) also studied MW-M31 pairs in numerical simulations finding the typical quantities characterizing the orbital parameters of the LG are rare among typical pairs, but not enough to challenge the ΛCDM model.

je.forero@uniandes.edu.co

Another definition of LG analogues is made by Li & White (2008), but despite differences ocurr in the definitions and resulting fraction of LG analogues, all are in agreement with a low frequency of these pairs.

To better understand the properties of the LG and how this uncommon pair configuration fit in the cosmological context, an immediate question arise. What else can we say of the LG at larger scales?. In particular, which are the typical/prefered locations of these systems within the Cosmic Web?. To what extent is this an expected configuration in ΛCDM.

Looking the LG at larger scales we have it is located in a difuse and warped filament/wall conecting Virgo Cluster with Fornax Cluster, some nearby galaxies and groups members of this large structure are the Maffei group, NGC 6744, NGC 5128, M101, M81, NGC1023, Cen A group. At this scale, there is no evident alignment of the MW-M31 orbital plane with the local filament or the Virgo-Fornax direction. However, if we look in a smaller volume below scales of ~ 6 Mpc, there is a clear alignment of th the MW-M31 orbit with a local plane as shown by Figure 3 in Courtois et al. (2013).

In this paper we study the large scale environment of LG analogues in the context of ΛCDM. We use the Bolshoi simulation to explore in what structures they reside and if there is any correlation or alignment with the cosmic web. The large scale Environment is defined by the cosmic web components identified by Forero-Romero et al. (2009), and we use the LG analogues computed by González et al. (2013a). We pay spetial attention to quantify the kind of environment that hosts LG pairs and their alignments with respect to the prefered directions defined by the T-web.

This paper is organized as follows. In Section 2 we present the N-body cosmological simulation and the algorithm to define the cosmic web, next in 3 we describe

the sample of LG analogues extracted from the simulation. In Section 4 we presents our results to continue with a discussion about their implications for our Local Group in Section 5 to finally conclude in Section 6.

2. SIMULATION AND WEB FINDING ALGORITHM

2.1. *The Bolshoi simulation*

We use the Bolshoi simulation of ΛCDM cosmology: $\Omega_{\rm m} = 1 - \Omega_\Lambda = 0.27$, $H_0 = 70\,{\rm km/s/Mpc}$, $\sigma_8 = 0.82$, $n_s = 0.95$ (Klypin et al. 2011), compatible with the constraints from the WMAP satellite (Hinshaw et al. 2013). The simulation followed the evolution of dark matter in a $250h^{-1}$Mpc box with spatial resolution of $\approx 1h^{-1}$ kpc and mass resolution of $m_{\rm p} = 1.35 \times 10^8$ M$_\odot$. Halos are identified with the BDM algorithm (Klypin & Holtzman 1997). The BDM algorithm is a spherical overdensity halo finding algorithm and is designed to identify both host halos and subhalos.

2.2. *Cosmic web identification*

The web finding algorithm is based on the tidal tensor computed as the Hessian of the gravitational potential field

$$T_{ij} = \frac{\partial^2 \phi}{\partial r_i \partial r_j}, \quad (1)$$

where r_i, $i = 1, 2, 3$ refers to the three spatial comoving coordiates and ϕ is the gravitational potential renormalized to follow the Poisson equation $\nabla^2\phi = \delta$ where δ is the matter overdensity.

This tensor is real and symmetric, which means that can be diagonalized. We note its eigenvalues as $\lambda_1 \geq \lambda_2 \geq \lambda_3$ and their corresponding eigenvectors $\hat{e}_1$, $\hat{e}_2$ and $\hat{e}_3$. The web classification compares each one of the three eigenvalues to a threshold value $\lambda_{\rm th}$. If the three, two, one or zero eigenvalues are larger than this threshold the region is classified as peak, filament, sheet or void, respectively.

Forero-Romero et al. (2009) performed a detailed study for the topology of the cosmic web and its visual counterpart as a function of the parameter $\lambda_{\rm th}$. They found that reasonable results in terms of the volume fraction occupied by voids, the visual inspection and the halo populations in each web type can be reached by values of $0.2 < \lambda_{\rm th} < 0.4$. In this paper we choose the value of $\lambda_{\rm th} = 0.3$ to proceed with our analysis. This is only relevant to the classification of the simulation into web elements. Other results are completeley independent of this choice. Nevertheless we have checked that the main conclusions of this work do not depend on the choise of $\lambda_{\rm th}$.

The algorithm to compute the potential is grid based. First we interpolate the density into a cubic grid with a Cloud-In-Cell (CIC) scheme and smooth it with a gaussian kernel. Then we obtain the gravitational potential using FFT methods and use finite differences to compute the Hessian at every point in the grid. In our case we have used a grid size on and a gaussian smoothing with two times larger as the typical separation between the two halos in the Local Group. The purpose of this choice is to have both halos in the pair a common environment. In this paper we use a grid spacing of $s = 0.97$ h^{-1}Mpc , corresponding to a 256^3 grid in the Bolshoi volume. The scale for the gaussian smoothing uses the same value.

We use the matter overdensity, ellipticity and the prolatenes to further characterize the web. These quantities are defined in terms of the eigenvalues as follows

$$\delta = \lambda_1 + \lambda_2 + \lambda_3, \quad (2)$$

$$e = \frac{\lambda_3 - \lambda_1}{2(\lambda_1 + \lambda_2 + \lambda_3)}, \quad (3)$$

$$p = \frac{\lambda_1 + \lambda_3 - 2\lambda_2}{2(\lambda_1 + \lambda_2 + \lambda_3)}. \quad (4)$$

We also measure the alignment of the LG halos with respect to the cosmic web defined by the eigenvector. To this end we characterize each LG pair by two vectors. The first is $\hat{n}$, the vector marking the axis along the orbital angular momentum of the pair, normal to its orbital plane; the second is $\hat{r}$, the vector that connects the halos in the pair which can be related to the alignment of the radial velocities to the web. We quantify the alignment using the absolute value of the cosinus of the angle between the two vectors of interest $\mu = |\hat{e}_i \cdot \hat{n}|$ or $\mu = |\hat{e}_i \cdot \hat{r}|$, where $i = 1, 2, 3$.

The data of the BDM halos and the Tweb is publicly available through a database located at http://www.cosmosim.org/. A detailed description of the database structure was presented by Riebe et al. (2013).

3. LOCAL GROUP ANALOGUES

To construct a sample of the MW-M31 pairs at $z \approx 0$, we use a series of simulation snapshots at $z < 0.1$ (since the last ≈ 1.3 Gyr) spaced by $\approx 150 - 250$ Myr. This is done because a particular configuration of MW and M31 is transient and corresponds to a relatively small number of systems at one snapshot. By using multiple snapshots we can increase the sample of systems in such configuration during a period of time in which secular cosmological evolution is small.

The LG analogues or General Sample (GS) in this paper are pairs selected in relative isolation, and in a wide range of masses from $M_{200c} = 5{\times}10^{11}$ M$_\odot$ to $5{\times}10^{13}$ M$_\odot$. Isolation criteria includes a pair closer than 1.3Mpc, and with no massive neighbors within 5Mpc. In addition we require that pairs have no Virgo-like neighbor halo with mass $M_{200c} > 1.5 \times 10^{14}$ M$_\odot$ within 12 Mpc. We have 5480 pairs under these general criteria. A full description of the selection criteria can be found in González et al. (2013a,b).

We also define two subsamples more closely related to the MW-M31 dynamics according to the tolerance in additional constraints. A sample named 2σ, correspondig to LG analogues constrained by two times the observational errors in the orbital values (radial velocity, tangential velocity, and separation), and a more relaxed sample named 3σ for LG analogues constrained by three times observational errors accordingly. The number of pairs in each sample is 46 and 120 respectively, notice we have less pairs than in González et al. (2013a) results, since we removed pairs which are too close at $z = 0$, i.e. their virial radii overlaps, also we removed a couple pairs that

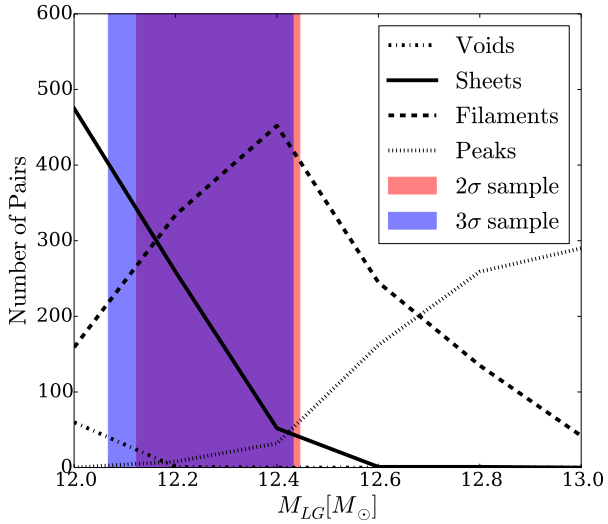

FIG. 1.— Mass distribution of pairs in the different environments for the general sample. The shaded regions show the mass ranges of 2σ and 3σ samples.

merged or change their mass more than 20% at present time since they were detected at $z < 0.1$.

4. RESULTS

4.1. *The prefered environment for LGs*

The first result we explore is the kind of environment occupied by our LGs. We find that the LGs in the general sample are located across all different evironment without any strong preferences; 1/3 are located in sheets, 1/4 in peaks, 1/4 in filaments and the remaning 1/6 in voids.

The situation in the restricted 2σ and 3σ samples is very different. By large the LGs in these samples are located in filaments and sheets. In both samples, $\sim 50\%$ of the pairs can be found in filaments while $\sim 40\%$ are in sheets. These absolute numbers in each environment for each sample are presented in Table 1.

This difference between the general and the restricted samples is due the mass ranges covered by each sample. In González et al. (2013a) the mass range covered by 2σ and 3σ is very narrow and it is used to constraint the LG mass. We show in table 1 that subset of the GS having a similar mass range to 2σ and 3σ reproduces similar environment fractions.

Figure 1 clearly shows the correlation between environment an total pair mass. Each line represents the mass distribution of pairs in the four different environments for the general sample. High mass pairs tend to be located in peaks and filaments while less massive ones in voids and sheets. The shaded regions represent the 68% confidence intervals of the mass distributions of 2σ and 3σ samples.

4.2. *Web Overdensity, Ellipticity and Anisotropy*

We now describe the preferred place of the LG samples in terms of the web overdensity, ellipticiy and anisotropy as defined in Section 2.

Figure 2 shows dependency of the web overdensity, ellipcitiy, and prolateness on pair mass for the different samples. GS is represented by the solid lines with the associated errors covered by the shaded region. The symbols represents the results for the 2σ and 3σ samples. In all cases it is immediatly clear that the range of values for the 2σ and 3σ samples are completely expected from its mass dependence.

Left panel shows the overdensity dependence on pair mass. Higher mass pairs are located in high density regions. The 2σ and 3σ samples having a narrower mass range as shown in previous figure, are consequently located within a narrower range of overdensities $0.0 < \delta < 4.0$ peaking at $\delta \sim 1$. This is also consistent with the fact that these samples are mostly found in filaments and sheets. The average overdensity of 2σ and 3σ samples is expected from the values in the GS within the same mass range.

Middle and right panels show web ellipcitiy and absolute prolateness dependence on mass. Again we noticed that within the same mass range, the 2σ and 3σ average ellipcitiy and prolateness does not differ significantly from GS For the 2σ and 3σ samples most of the pairs are located in a narrow range for ellipticities in the range $0.1 < e < 1.0$, and prolateness $|p| < 0.5$.

4.3. *Alignment along the cosmic web*

We now study the alignment of the LG with respect to the cosmic web.

4.3.1. *Orbital Angular Momentum*

Figure 3 and 4 show the main result of that study. They present the cumulative distribution of $\mu \equiv \hat{e}_i \cdot \hat{n}$ and $\mu \equiv \hat{e}_i \cdot \hat{r}$ for the three eigenvectors $i = 1, 2, 3$. Lines in each panel correspond to different samples. The straight line across the diagonal shows the expected result for vectors with randomly distributed directions.

For the alignment of $\hat{n}$ in Figure 3 there are two important features. First the alignments themselves. There is a strong anti-alignment signature between $\hat{n}$ and the third eigenvector. With respect to the second eigenvector the distribution is consistent with no aligment. For the first eigenvector there is a strong alignment, an expected result after considering the results with the other eigenvectors and keeping in mind that the eigenvectors are orthonormal. Second, the alignment strenght changes for the different samples. For the anti-alignment with $\hat{e}_3$ the signal strenghtens as we move from the GS to the 3σ into the 2σ sample.

Quantitatively, the anti-alignment feature found with the $\hat{e}_3$ vector means that for 2σ sample, $\sim 50\%$ pairs have $|\mu| < 0.2$ (78 degrees angle), and $\sim 75\%$ pairs have $|\mu| < 0.4$ (66 degrees angle). These signals do not change significantly on different environments as has been already show in different alignment studies that similar (Libeskind et al. 2013) or identical (Forero-Romero et al. 2014) web finding techniques as ours. In particular these trends hold for pairs in filaments and walls. If we consider only pairs in filaments, we have that the pair orbital angular momentum tends to be perpendicular to the filament direction, in the case of sheets it tends to lie within the sheet plane.

Can the increase of the alignment strenght in the different samples be explained as a consequence of different mass dependencies as the results in the previous section?

Sample	Peak	Filament	Sheet	Void
	n (%)	n (%)	n (%)	n (%)
2σ	4 (8.7)	24 (52.2)	17 (36.7)	1 (2.2)
3σ	10 (8.3)	58 (48.3)	47 (39.2)	5 (4.2)
General	1312 (23.9)	1472 (26.9)	1769 (32.3)	927 (16.9)
General ($12.1 < \log_{10} M_{\rm LG}/{\rm M}_\odot < 12.3$)	8 (1.4)	334 (55.5)	259 (43.0)	1 (0.1)

TABLE 1
Number of pairs in the four different kinds of environments for each of the three samples presented in Section 3. In parethesis the same number as a percentage of the total population. The last line in the table corresponds to the general sample with an additional mass cut for the total pair mass.

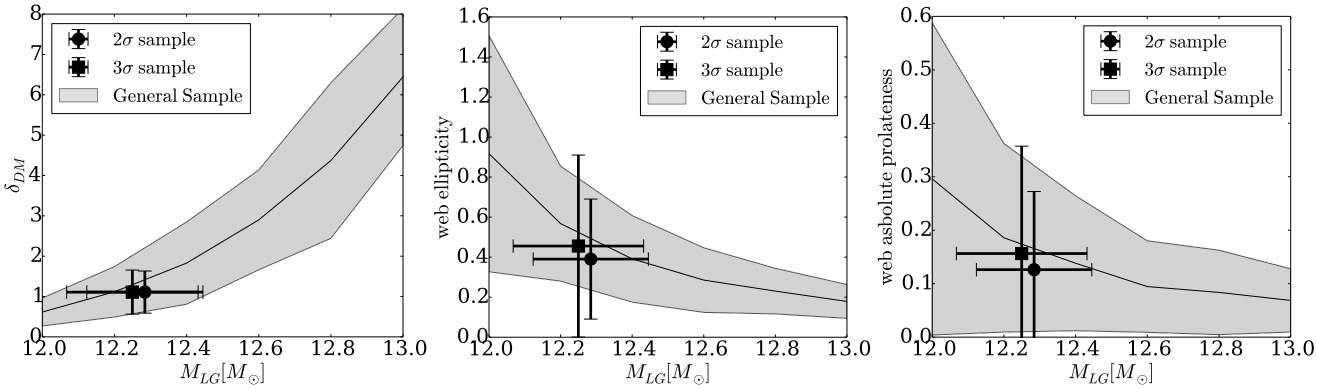

Fig. 2.— Mass dependency of the average dark matter overdensity (left), web ellipticity (middle) and web absolute value prolateness (right) at the pair location.

No. In Figure 5 we show the median of $\mu \equiv \hat{e}_i \cdot \hat{n}$ in different total mass bins. Lines show the median μ-mass relation for the three eigenvectors in the GS, Dots represent the results for the 2σ-3σ samples. In a mass range around $1.5 - 2.0 \times 10^{12}$ M$_\odot$the median of μ decreases as we increase the constraints on the pairs, not as a result of narrowing mass selection.

4.3.2. *Radial motion*

For the alignment of $\hat{r}$ in Figure 4 there are similar features as in the case of $\hat{n}$. In this case we find that the vector $\hat{r}$ is strongly aligned along the direction defined by $\hat{e}_3$ and anti-aligned along $\hat{e}_1$; correspondingly the signal along $\hat{e}_2$ is rather weak.

In this case we also find a stronger signal as we move into more restrictive samples, although the signal from the GS is already very significant. Quantitatively, the alignment feature with $\hat{e}_3$ means that for the 2σ and 3σ samples, $\sim 50\%$ pairs have $|\mu| > 0.8$ (36 degrees angle) and $\sim 25\%$ pairs have $|\mu| < 0.95$ (18 degrees angle).

Considering that the 2σ and 3σ samples move primarely along the radial direction, we can say that the motion of the LG halos is mostly done along the $\hat{e}_3$ vectors, consistent with recent results that report a strong alignment of halo's peculiar velocities along that direction (Forero-Romero et al. 2014).

4.3.3. *Halo Spin*

We also explore the alignment of the angular momentum (spin) of each pair member $\hat{j}_A$ and $\hat{j}_B$ with each other, the orbital angular momentum and with the cosmic web.

Figure 6 shows the cumulative distribution of dot product between angular momentum of the two halos. We find a a slight alignment of spin vectors for the 2σ sample with a median aroung $|\mu| \sim 0.7$ (45 degrees) However, we found no significant alignment with the orbital angular momentum or the cosmic web.

In the LG, the angle between MW and M31 spin is $\sim 60^\circ$ ($|\mu| = 0.5$) and the angles between spins and orbital angular momentum are $\sim 33^\circ$ ($|\mu| = 0.83$) and $\sim 76^\circ$ ($|\mu| = 0.24$) for MW and M31 respectively (van der Marel et al. 2012a). Consistent with our results of no particular alignement.

5. DISCUSSION

We explored the characteristics of the LG location in the cosmic web.

LG pairs are preferentially located in filaments and sheets. The mass range of the pairs sample plays an important role in the fractions for each environment type as shown in table 1 and figure 1.

There is a clear anti-alignment between the third eigenvector and the vector normal to the pair orbital plane. This feature is not mass dependant as can be shown in figure 3. For pairs in filaments this means the pair orbit tends to be perpendicular to the filament direction, and both pair members lie along the filament, and in the case of pairs in sheets, we have the pair orbital plane lie in the sheet plane. We also found this anti-alignment becomes stronger for the samples being more closely related to the LG, it means it is stronger for 2σ sample. All these alignment features are consistent with pair orbits relaxing their movements towards the slowest collapsing directions at larger scales.

LG pairs are located in a narrow range of local overdensity, ellipciticy and prolateness. And this is consistent with the narrow mass range selection of specific samples.

The LG spin and orbital angular momentum have no

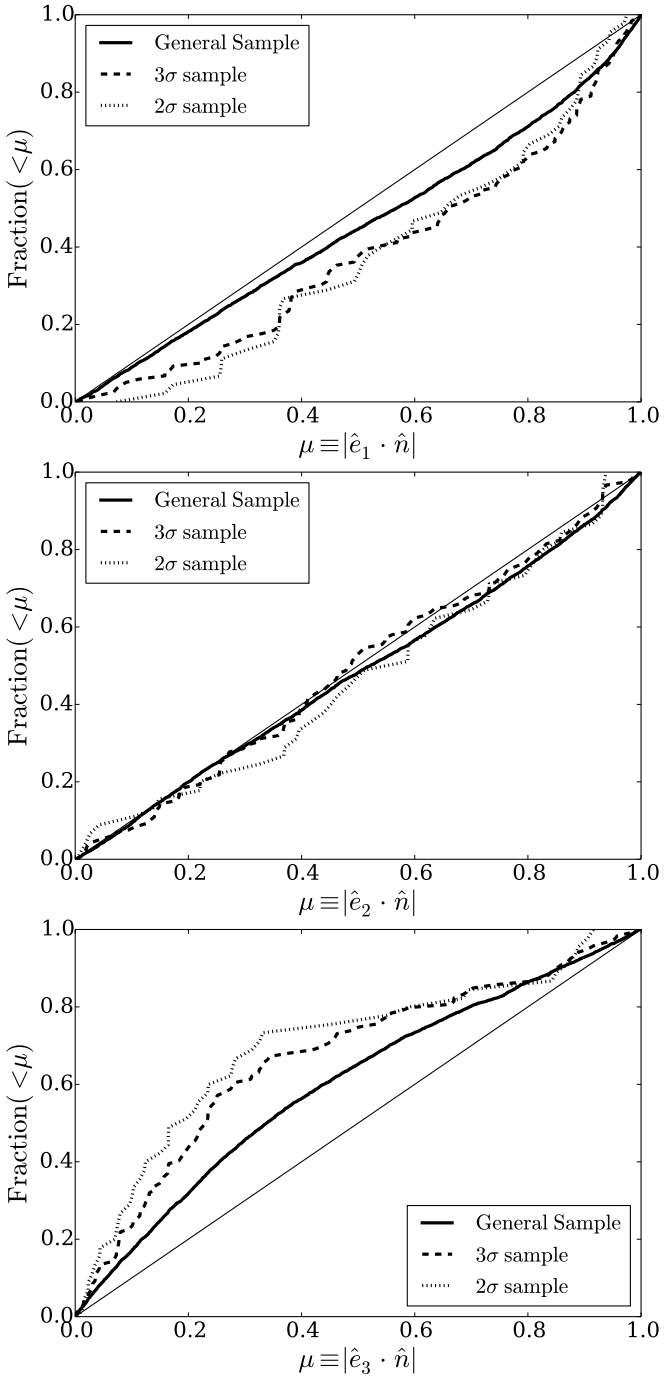

FIG. 3.— Cumulative distributions for the alignment between the normal vector to the pair orbital plane, $\hat{n}$, and the three eigenvectors in the Tweb.

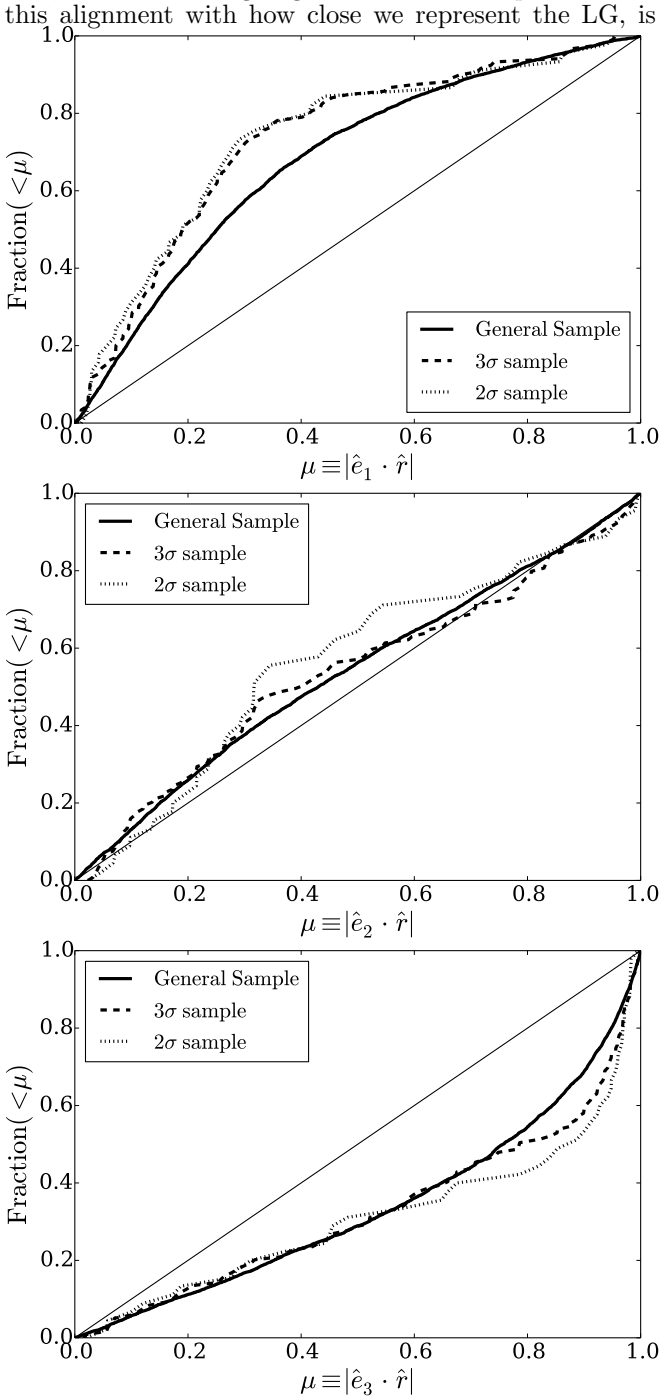

FIG. 4.— Cumulative distributions for the alignment between the vector linking the two halos in the pair, $\hat{r}$, and the three eigenvectors in the Tweb.

particular alignment, and we see no significan alignments in our LG pairs, however for the alignment between pair spins we found a slight alignment signature for 2σ sample as can be seen in figure 5.

These alignment features are in agreement with the scenario that pairs created in-situ or falling into a filament/wall align their orbits with the large scale structure in a relaxation process where pair members tend to moves along the slowest collapsing directions. However, the most intriguing feature is the dependence of this alignment with how close we represent the LG, is still not clear. We explore if the pair masses are responsible of this, but we found no dependence at all.

6. CONCLUSIONS

ACKNOWLEDGEMENTS

REG was supported by Proyecto Financiamiento Basal PFB06 and Comite Mixto ESO.

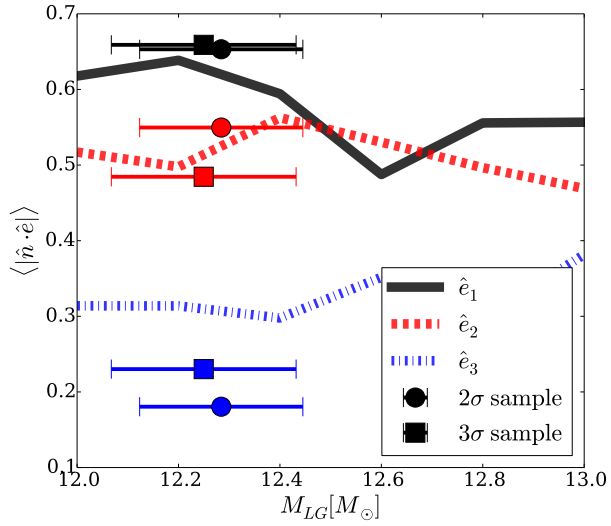

FIG. 5.— Mass dependency of the median value for the dot product between the normal vector $\hat{n}$ and each one of the eigenvectors. The lines show the trends for the general sample.

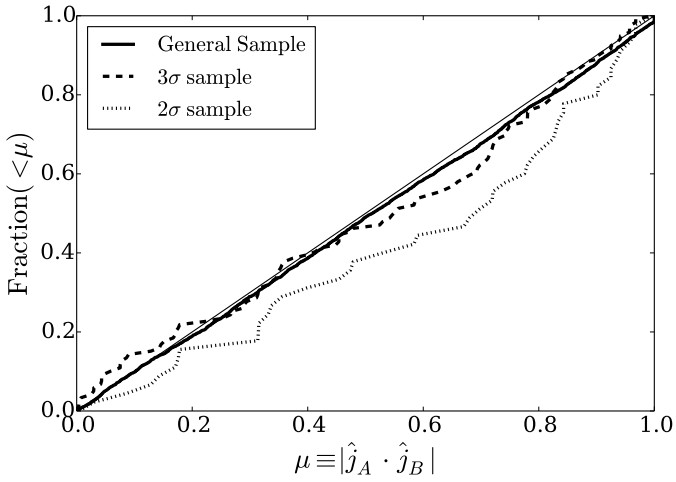

FIG. 6.— Alignment between the two angular momentum vectors of the two halos in the pair.

REFERENCES

Aragon-Calvo, M. A., Silk, J., & Szalay, A. S. 2011, MNRAS, 415, L16

Courtois, H. M., Pomarède, D., Tully, R. B., Hoffman, Y., & Courtois, D. 2013, AJ, 146, 69

Cox, T. J., & Loeb, A. 2008, MNRAS, 386, 461

Forero-Romero, J. E., Contreras, S., & Padilla, N. 2014, ArXiv e-prints

Forero-Romero, J. E., Hoffman, Y., Bustamante, S., Gottlöber, S., & Yepes, G. 2013, ApJ, 767, L5

Forero-Romero, J. E., Hoffman, Y., Gottlöber, S., Klypin, A., & Yepes, G. 2009, MNRAS, 396, 1815

González, R. E., Kravtsov, A. V., & Gnedin, N. Y. 2013a, ArXiv e-prints

—. 2013b, ApJ, 770, 96

Hinshaw, G., Larson, D., Komatsu, E., Spergel, D. N., Bennett, C. L., Dunkley, J., Nolta, M. R., Halpern, M., Hill, R. S., Odegard, N., Page, L., Smith, K. M., Weiland, J. L., Gold, B., Jarosik, N., Kogut, A., Limon, M., Meyer, S. S., Tucker, G. S., Wollack, E., & Wright, E. L. 2013, ApJS, 208, 19

Karachentsev, I. D. 2005, AJ, 129, 178

Klypin, A., Hoffman, Y., Kravtsov, A. V., & Gottlöber, S. 2003, ApJ, 596, 19

Klypin, A., & Holtzman, J. 1997, ArXiv Astrophysics e-prints

Klypin, A. A., Trujillo-Gomez, S., & Primack, J. 2011, ApJ, 740, 102

Li, Y.-S., & White, S. D. M. 2008, MNRAS, 384, 1459

Libeskind, N. I., Hoffman, Y., Forero-Romero, J., Gottlöber, S., Knebe, A., Steinmetz, M., & Klypin, A. 2013, MNRAS, 428, 2489

Mei, S., Blakeslee, J. P., Côté, P., Tonry, J. L., West, M. J., Ferrarese, L., Jordán, A., Peng, E. W., Anthony, A., & Merritt, D. 2007, ApJ, 655, 144

Riebe, K., Partl, A. M., Enke, H., Forero-Romero, J., Gottlöber, S., Klypin, A., Lemson, G., Prada, F., Primack, J. R., Steinmetz, M., & Turchaninov, V. 2013, Astronomische Nachrichten, 334, 691

Sandage, A., & Tammann, G. A. 1975, ApJ, 196, 313

Sohn, S. T., Anderson, J., & van der Marel, R. P. 2012, ApJ, 753, 7
van der Marel, R. P., Besla, G., Cox, T. J., Sohn, S. T., & Anderson, J. 2012a, ApJ, 753, 9
van der Marel, R. P., Fardal, M., Besla, G., Beaton, R. L., Sohn, S. T., Anderson, J., Brown, T., & Guhathakurta, P. 2012b, ApJ, 753, 8